

Disclosure of Domain Structure in Cubic $\text{Ca}_x\text{Zr}_{1-x}\text{O}_{2-x}$, $0.15 \leq x \leq 0.20$, by Talbot Image Enhancement of High-Resolution Electron Micrographs

BY H. J. ROSSELL

CSIRO Division of Materials Science and Technology, Locked Bag 33, Clayton 3168, Victoria, Australia

J. R. SELLAR

Department of Materials Engineering, Monash University, Clayton 3168, Victoria, Australia

AND I. J. WILSON

CSIRO Division of Materials Science and Technology, Locked Bag 33, Clayton 3168, Victoria, Australia

(Received 28 February 1991; accepted 1 July 1991)

Abstract

High-resolution electron microscope images have been recorded of several crystalline samples of calcia-stabilized zirconia (Ca-CSZ) and of the fluorite-related superstructure phase φ_1 (CaZr_4O_9). The contrast of the CSZ images has been enhanced markedly by the light-optical Talbot self-imaging technique. It is demonstrated that the CSZ crystals contain a coherent dispersion of microdomains approximately 30 Å in diameter, and that the structure of the microdomains is that of φ_1 .

Introduction

Zirconia (ZrO_2) may be alloyed with oxides such as CaO, MgO or Y_2O_3 to form a solid-solution phase known as cubic stabilized zirconia (CSZ) which is of considerable importance in ceramic and solid electrolyte technology. The phase is stable over extended ranges of temperature and composition (Levin & McMurdie, 1975). Phase relationships in the CaO– ZrO_2 system are shown in Fig. 1. Although the cubic $\text{Ca}_x\text{Zr}_{1-x}\text{O}_{2-x}$ phase (Ca-CSZ) decomposes eutectoidally below about 1500 K, in practice it may be retained at room temperature by reasonably fast cooling, since solid-state reactions occur quite slowly. The compounds φ_1 and φ_2 are the fluorite-related superstructure phases CaZr_4O_9 and $\text{Ca}_6\text{Zr}_{19}\text{O}_{44}$ known to exist in this system (Michel, 1973; Hellmann & Stubican, 1983); these can be expected to have the same structures as those of CaHf_4O_9 and $\text{Ca}_6\text{Hf}_{19}\text{O}_{44}$ (Allpress, Rossell & Scott, 1975) in view of the close similarity in electron and X-ray diffraction data of the corresponding Zr and Hf compounds and of the known similarity in chemical behaviour of Zr and Hf.

It has become widely accepted that stabilized zirconia has the f.c.c. fluorite (CaF_2) structure, with

the Zr and solute metal atoms distributed randomly on all the available cation sites, and with the deficiency of oxygen with respect to the ideal MO_2 stoichiometry accommodated as a random distribution of vacant anion sites. This description is in accord with the results of density measurements and of structure refinements based on measurements of diffracted X-ray intensities (Filatov & Frank-Kamenetskii, 1969; Morinaga, Cohen & Faber, 1979), and accounts for the property, characteristic of the phase, that anionic movement (diffusion, conductivity) is rapid even at relatively low temperatures, whereas cationic movement is slow and occurs only at high temperatures (Etsell & Flengas, 1970).

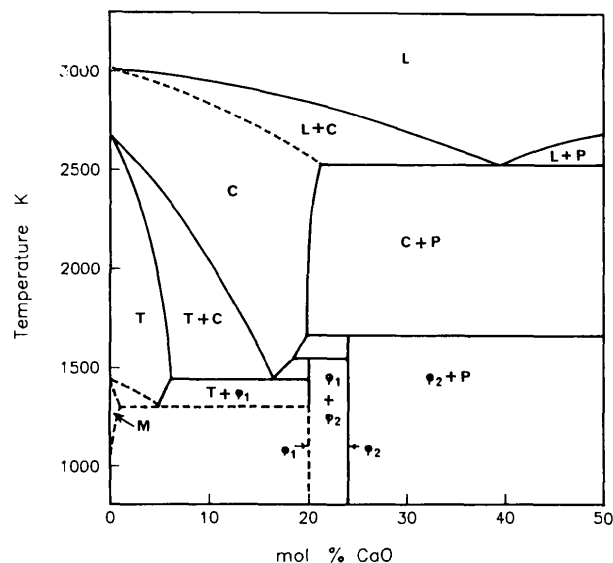


Fig. 1. Equilibrium phase diagram for the system CaO– ZrO_2 after Hellmann & Stubican (1983). The regions are: C, CSZ phase; T and M, tetragonal and monoclinic ZrO_2 (solid-solution) phases; P, perovskite CaZrO_3 ; L, liquid; φ_1 , CaZr_4O_9 ; φ_2 , $\text{Ca}_6\text{Zr}_{19}\text{O}_{44}$.

The departure from the ideal MO_2 stoichiometry of the phase is such that about one in ten of the anion sites may be formally vacant. The anion sublattice of fluorite is primitive cubic (of half the fluorite cell edge): a random distribution of vacancies on this lattice at a concentration of ~ 0.1 would mean that vacancies generally would be at first and second nearest-neighbour distances from one another. Therefore it is probable that relaxation and ordering effects occur in the anion substructure: the non-linear variation of anionic conductivity of Ca-CSZ with CaO content has been attributed to such effects (Carter & Roth, 1968). The most direct evidence for ordering effects comes from diffraction studies: diffuse reflexions are obtained in addition to the sharp Bragg reflexions expected from the fluorite structure, and these are particularly evident in single-crystal electron diffraction patterns. For the cubic phase in different chemical systems (e.g. CaO-ZrO₂, Y₂O₃-ZrO₂, Y₂O₃-Ta₂O₅), patterns from a given orientation display similar diffuse features, but the relative proportions of such features differ between the various systems, suggesting that the ordering details differ as well (Rossell, 1981). For a given crystalline orientation in any one system, the diffuse pattern does not vary if the composition is changed within broad limits; for example electron diffraction patterns from $Ca_xZr_{1-x}O_{2-x}$ are the same, apart from possible overall intensity differences, for $0.12 \leq x \leq 0.2$. It can be estimated from the widths of the diffuse features that they arise from regions of about 30 Å diameter within a crystal, and dark-field images formed in the electron microscope with beams corresponding to a diffuse feature are mottled on this scale (Allpress & Rossell, 1975).

Interpretations of this diffuse scattering in the particular case of Ca-CSZ have differed fundamentally in approach. Morinaga, Cohen & Faber (1980) assumed that the structure of cubic $Ca_xZr_{1-x}O_{2-x}$ was basically that of fluorite with vacant anion sites, that the crystalline environment at each lattice point was the same, on average, and that the diffuse intensity arose from short-range order, size-effect, first-order thermal and Huang diffuse-scattering effects. They were able to obtain values for the various parameters in their scattering equation from a least-squares fit of calculated and observed X-ray intensities.

Allpress & Rossell (1975) used a model for the phase $Ca_xZr_{1-x}O_{2-x}$ and the closely similar HfO₂-based material in which it was assumed that the atomic positions throughout a crystal were those of fluorite: the metal atoms and formally vacant oxygen sites, however, were not distributed randomly, but were ordered according to the scheme exhibited in the fluorite-related superstructure $\varphi_1 [Ca(Zr,Hf)_4O_9]$, but only in discrete regions or microdomains some

30 Å in diameter. As twelve orientations of the φ_1 ordering pattern are possible for a given orientation of the basic fluorite-type structure, it was assumed that equal numbers of microdomains occurred in all such orientations. The observed electron diffraction patterns could be matched with those calculated from this model using atomic parameters for φ_1 from a partial structure determination (Allpress, Rossell & Scott, 1975). Crystals of overall composition 20 mol% Ca would consist entirely of microdomains, whereas in material of lower overall Ca content, the CaZr₄O₉ microdomains will be further apart and separated by a strained but coherent fluorite matrix of relatively low Ca and vacancy content.

This model explains the invariance of the diffuse scattering with varying Ca content of the specimen, noted above, and the non-linear variation in anionic conductivity with increasing concentration of formal anion vacancies in Ca-CSZ (Rossell, 1981). The validity of the microdomain model was supported by the observation that on appropriate annealing, the size of the microdomains gradually increased (with consequent gradual sharpening of the diffuse electron diffraction features into festoons of spots, the positions and intensities of which could be matched by calculation) until they were of sufficient size to be identified unambiguously as φ_1 from single-crystal electron diffraction patterns.

Diffuse X-ray diffraction intensities calculated from the microdomain model, and based on the original partially determined structure for φ_1 (Allpress, Rossell & Scott, 1975), do not agree with those observed by Morinaga, Cohen & Faber (1980), although there is agreement in the position of diffuse peaks. However, such calculations based on a more recent complete structure for CaZr₄O₉ determined and refined from powder neutron and X-ray diffraction data (to be published) are in essential agreement with the observations of Morinaga, Cohen & Faber (1980) at least for the small area of the [110] section of reciprocal space that they published.

A serious inconsistency distinguishes the two models. According to the microdomain description of Ca-CSZ, essentially all the Ca atoms are in microdomains of φ_1 structure: this constrains the Ca atoms to be coordinated by the full complement of eight O atoms and the formal anion vacancies to be nearest neighbours to Zr atoms only. Such a prohibition on formal vacancies and Ca atoms as nearest neighbours is supported by the calculations of Dwivedi & Cormack (1990). However, Morinaga, Cohen & Faber (1980) deduce from the values of their short-range-order coefficients that, on average, anion vacancies tend to be nearest neighbours to Ca rather than Zr.

More recently, a study of the diffuse neutron scattering from a single crystal of $Ca_{0.15}Zr_{0.85}O_{1.85}$

has been made by Neder, Frey & Schulz (1990). Their interpretation is that two types of defect are distributed in a correlated way on the atomic positions of the fluorite structure; one defect is a single oxygen vacancy with relaxed neighbouring ions and the other a pair of oxygen vacancies separated by a $\frac{1}{2}(111)$ fluorite vector with a Ca ion in between. This model was refined to give a satisfactory agreement of observed and calculated diffuse intensity. However, an excellent match of their observed (and calculated) diffuse neutron scattered intensity also can be made with that calculated from microdomains of φ_1 structure of about 20 Å diameter. The two models cannot be made equivalent (*e.g.* by averaging the microdomain constitution over the whole crystal), since there remains the fundamental conflict whether or not the Ca is associated with nearest-neighbour oxygen vacancies.

In the present work, a decision between these models is attempted using high-resolution electron microscopy. The outcome is an apparent confirmation of the φ_1 microdomain description, but no resolution of the inconsistency with the alternative structural models is afforded.

Experimental procedures

Materials

Alloys $\text{Ca}_x\text{Zr}_{1-x}\text{O}_{2-x}$, $x = 0.12, 0.15, 0.17, 0.18$ and 0.20 , were prepared from CaCO_3 (BDH analytical reagent, pre-fired at 770 K) and ZrO_2 (Ugine-Kuhlmann Hf-free grade, pre-fired at 1250 K). Weighed quantities of these powders were milled together under acetone in a boron carbide mortar, pressed into small (~ 0.3 g) pellets and reacted at 1250 K for 1 h. These were reground and repelleted, then either fired at 1970 K in air for several days to form the desired cubic stabilized zirconia phase and quenched in water, or melted and quenched from the melt. In the latter case, melting was done either in argon on the water-cooled hearth of an arc furnace or in air in a solar furnace. Materials that had been arc-melted were initially black because of partial reduction in the argon atmosphere, but these could be restored to a colourless condition by heating in air at 1100 K for 10 min or so. Equivalent materials prepared by all of these routes showed no differences in diffraction properties.

Powder X-ray diffraction photographs of all specimens were taken using a Hägg–Guinier focussing camera and with thoria ($a_o = 5.5970$ Å) as an internal standard. Lattice parameters were determined from these using a least-squares procedure and assuming for the weighting scheme that the positions of all lines could be measured with equal precision. The lattice parameters varied

linearly with composition from 5.1328 (2) Å for $x = 0.15$ to 5.1402 (2) Å for $x = 0.20$. Specimens with $x = 0.12$ [$a_o = 5.1300$ (3) Å] invariably contained a trace of ZrO_2 , but all the others were single-phase cubic material, according to the powder patterns.

A specimen of φ_1 (CaZr_4O_9) was made by reacting mixed powders of 20 mol% CaO content initially at 1250 K, as above, then heating the product in air at 1420 K for 6 months, during which annealing time, φ_1 crystallites grew to ~ 0.5 μm diameter. The Guinier photographs of this material showed that it was a single phase. The φ_1 superstructure is monoclinic, space group $C2/c$, and the axial relationship of the supercell to the fluorite-type subcell is $a = [222]$, $b = [220]$, $c = \frac{1}{2}[3\bar{3}2]$ (Allpress, Rossell & Scott, 1974). The lattice parameters of the CaZr_4O_9 specimen determined here were $a = 17.783$ (3), $b = 14.569$ (3), $c = 12.069$ (3) Å, $\beta = 119.42$ (2)°.

Electron microscopy

Specimens were crushed finely under ethanol and dispersed on grids coated with a holey carbon film. They were examined in a JEOL 200CX high-resolution electron microscope fitted with a top-entry specimen holder and $\pm 10^\circ$ double-tilt goniometer, and operated at 200 kV. Single-crystal fragments of suitable thickness and orientation were sought, and through-focal series of images recorded using an objective aperture of 2 \AA^{-1} diameter in the diffraction plane.

The computation of simulated images was carried out using the suite of programs *SHRLI* (O'Keefe & Buseck, 1979) which perform the multislice type of calculation incorporating the effects of dynamical scattering and microscope aberrations. The usual slice thickness was about 2 Å, and satisfactory values of normalized intensity sums were obtained for total thicknesses of up to 100 slices. Image calculations usually were carried through using those beams included in an aperture of 1 \AA^{-1} radius in the diffraction plane: however, structure factors and phase grating coefficients were extended to twice the scattering angle corresponding to this radius so as to make sure that all dynamical scattering effects were included correctly.

Optical processing

In most of the observed images of the cubic CaO-stabilized zirconia phase, the contrast effects of interest were difficult to see because they were feeble and superimposed on the expected lattice images of the cubic basis structure. In a few cases, however, optical enhancement procedures were feasible; these were carried out using an optical processor of novel design (Wilson, 1985) in which reflecting optical elements are used to produce a diffraction pattern

from an electron micrograph and to reconstruct the image.

A copy of the electron micrograph of appropriate overall density was made, using a unit-magnification projection-printing process. The copy was bleached, so that it behaved optically as a pure phase object. Such objects exhibit about a tenfold enhancement in diffraction efficiency in the non-zero order reflections compared with ordinary negatives which are amplitude objects: an important gain, since the diffraction effects of concern here were normally only marginally above the background level. This object was placed in the optical processor, and a binary mask was placed in the diffraction plane so as to pass only the beams of interest (*i.e.* the sharp spots due to the substructure and the visible diffuse features) and thereby filter from the input image most of the background and film grain noise. The perforations in the binary mask were of generous aperture, and placed so that their edges lay only in the background. Thus the convolute of the hole shape did not appear in the final image.

Light-optical images were recorded at the instrumental Gaussian focus, and for each object, 30–40 Talbot self-images* [*i.e.* Fourier images, in the terminology of Cowley & Moodie, (1960)] were recorded at regular 10 mm intervals of defocus. The original

* If a planar object with a periodic transmission function of repeat distance a is illuminated with parallel light, as is effectively the case for the optical device above, a series of images with the same intensity distribution as at the exit face of the object will appear at defects of focus $\Delta f = na^2/\lambda$, where n is an even integer, *i.e.* the spatial frequency is imaged with maximum contrast at these values of Δf . For n an odd integer, the image contrast is again at a maximum, but translated by half the periodicity (which amounts to a contrast reversal for cosine fringes), whilst for non-integral n , the image will be out of contrast.

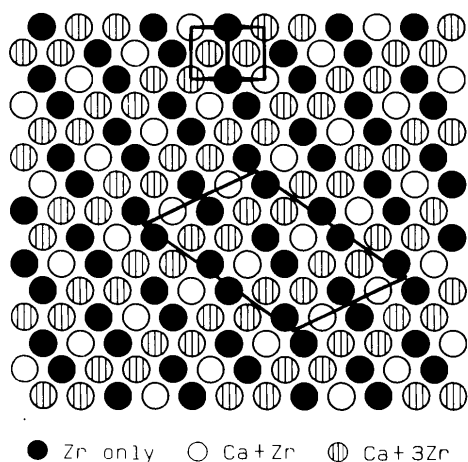


Fig. 2. Diagrammatic projection of φ_1 structure down $[010]$, showing cation positions only. The unit cells of φ_1 and of the fluorite substructure are outlined. 'Fringes' are visible at low angles of observation.

electron micrographs contained many different spatial frequencies, but those of particular interest were of very low amplitude. It was possible to find Talbot images at such defects of focus that these weak periodicities were at maximum contrast, whilst those of large amplitude were out of contrast or greatly attenuated. This technique therefore provided an extremely effective enhancement of the weak periodic features. A brief preliminary report of these results has been given (Rossell, Sellar & Wilson, 1986); further details of this and other allied optical processing techniques may be found in Wilson (1985).

Various other optical processing techniques that were tried produced less satisfactory results. These included (a) recording an image with a binary mask set to pass only the beams corresponding to the diffuse diffraction features, (b) superimposing an image formed as in (a) at long exposure on an unfiltered image of shorter exposure, and (c) a procedure as in (b), but using colour film and differently coloured light sources to produce the images.

Results and discussion

Satisfactorily resolved lattice images of the face-centred cubic phase $\text{Ca}_x\text{Zr}_{1-x}\text{O}_{2-x}$ were obtained at 200 kV if the orientation giving the most densely populated diffraction pattern, *viz.* $[110]$, was used. The majority of observations were made using this orientation, since image resolution in the next most favourable case, $[112]$, was marginal.

Images from φ_1

Since there was the possibility that atomic ordering occurs in the cubic phase according to the pattern exhibited in the fluorite-related superstructure φ_1 , through-focal series of high-resolution images were recorded for crystals of φ_1 from a well-characterized specimen. Interest was centred on images of φ_1 crystals which were oriented such that a direction of the form $\langle 110 \rangle$ for the nominally f.c.c. substructure was parallel to the beam, since then the substructure was resolved. Of the twelve such orientations of φ_1 that exist, it is only for $[010]$, $[0\bar{1}0]$, $[\bar{1}02]$ and $[10\bar{2}]$ (supercell indices) that supercell and subcell reflexions occur in the same reciprocal space plane; therefore only crystals in these four orientations would be expected to give images in which contrast effects due to the superstructure are superimposed on the substructure. Projected columns of atoms are differentiated as to type in these four orientations, an effect also reflected in the calculated projected crystal potential. This differentiation is much less marked for the $[\bar{1}02]$ and $[10\bar{2}]$ orientations, so that attention was confined to $[010]$ and

$[0\bar{1}0]$. A representation of the $[010]$ projection of φ_1 is shown in Fig. 2.

Simulated images of φ_1 were calculated using the structural information available for CaHf_4O_9 ; as noted above, it can be confidently expected that CaZr_4O_9 and CaHf_4O_9 are isostructural. In the determination and partial refinement of the Hf compound (Allpress, Rossell & Scott, 1975), metal-atom types

and their positional parameters were established, together with the most probable oxygen sites that are formally vacant; O atoms were left at their ideal fluorite-derived positions. For the present case, the same cation parameters were taken, but with Zr substituted for Hf, and it was assumed that those O atoms adjacent to the vacant sites had relaxed towards them from their ideal fluorite-type positions

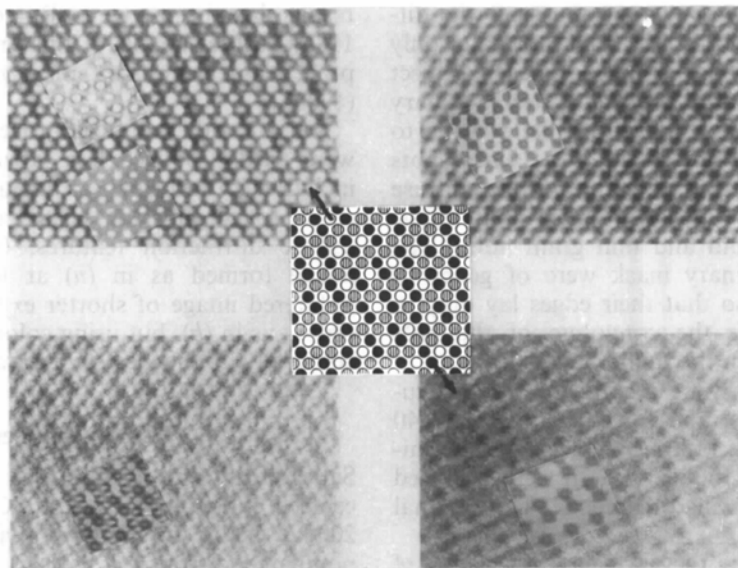


Fig. 3. Observed and calculated high-resolution images of φ_1 (CaZr_4O_9) in $[010]$ (supercell) orientation. The diagram of Fig. 2 is inset at the same scale. The 2-3 pattern (a row is arrowed) can be discerned with a variety of contrast changes. The values of crystal thickness and amount of defocus used in the calculations were (clockwise, from top right) 58, -550; 116, -658; 174, -658; 58, -700; and 58, -658 Å.

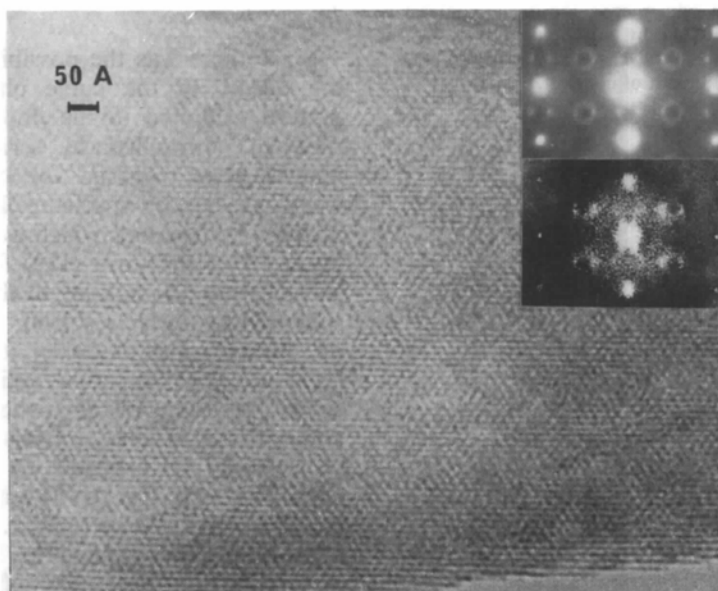


Fig. 4. High-resolution image from a crystal of $\text{Ca}_{0.17}\text{Zr}_{0.83}\text{O}_{1.83}$ in $[112]$ (cubic) orientation, with corresponding electron diffraction pattern and optical transform. These are typical of $[112]$ images and diffraction patterns from cubic material of all compositions. The substructure is poorly resolved, but a characteristic 'basketweave' pattern at about 30 Å suggests a microdomain constitution for the crystal.

by $\sim 0.2 \text{ \AA}$ so as to lie on the vertices of regular octahedra around the six-coordinated Zr atoms. This adjustment was considered to represent a closer approximation to the actual O-atom positions in the φ_1 structure as it was based on conditions that apply in all the other anion-deficient fluorite-related superstructures studied to date (Rossell, 1981); it caused only minor changes in the calculated intensities, however.

The calculated images varied rapidly with crystal thickness and amount of defocus. However, for thicknesses up to 200 \AA and defocus distances in the range -500 to -800 \AA , a characteristic pattern of alternating groups of two and three dots of differing contrast in rows parallel to the subcell direction $[1\bar{1}2]$ was often produced, which matched the observed image contrast under similar conditions (Fig. 3). This characteristic pattern, hereafter called the 2-3 pattern, also can be discerned in the simple projection of cation positions (Fig. 2), and therefore the group of two dots in this pattern may be taken to represent the Zr-only columns of atoms in projection. The 2-3 pattern could be recognized in the experimental images despite a variety of contrast changes and reversals which, as confirmed by calculation, were the result of variations in crystal thickness and amount of defocus (Fig. 3). Observed images not showing this characteristic pattern nevertheless displayed the symmetry of the unit cell of φ_1 in projection, and these could also be matched by calculated images. However, the 2-3 pattern was easily recognized, and was used most frequently to identify φ_1 in the appropriate orientation. Similar images, observed and simulated, have been produced by Shiojiri, Hirota, Isshiki, Maeda & Sekimoto (1988) in their study of evaporated CaO-ZrO₂ films.

Images from $\text{Ca}_x\text{Zr}_{1-x}\text{O}_{2-x}$

Electron microscope images from $\text{Ca}_{0.12}\text{Zr}_{0.88}\text{O}_{1.88}$ showed that the crystals were fragmented or consisted of numerous small regions separated by low-angle boundaries, an effect probably due to the separation of ZrO₂ in material of this composition. Attention was confined therefore to images from crystals of $\text{Ca}_x\text{Zr}_{1-x}\text{O}_{2-x}$, $0.15 \leq x \leq 0.20$.

Fig. 4 shows an unprocessed image of a CSZ crystal in the $[112]$ orientation and two representative unprocessed high-resolution $[110]$ images are shown in Fig. 5. There is a strong similarity between the electron diffraction patterns and the light-optical diffraction patterns from the electron micrographs (optical transforms): Fig. 5 also demonstrates an example of the (geometrical) invariance of the electron diffraction pattern with specimen composition.

The images in Fig. 5 show a $[110]$ projection of the f.c.c. structure resolved clearly down to the 3 \AA

spacing of dots running in rows parallel to $[1\bar{1}2]$ and $[1\bar{1}\bar{2}]$ (the two symmetrically equivalent sets of closest packed rows). Since there is a close similarity in the electron and optical diffraction patterns, the ordering effects that give rise to the diffuse electron diffraction features must be represented by contrast effects in the micrographs. Very weak modulations in the contrast of the dots occur over small regions of about 30 \AA diameter, the size indicated by the widths of the diffuse spots in both the optical and electron diffraction patterns. These modulations appear as sets of faint fringes occurring in patches over the image, with directions and spacings corresponding to the four pairs of diffuse spots in the optical transform, and are identical to the contrast fringes seen in equivalent directions in the diagrammatic $[010]$ projection of φ_1 (Fig. 2) and its mirror image. The 2-3 pattern occurs in the contrast of the dots in most of the $[110]$ images from all materials $\text{Ca}_x\text{Zr}_{1-x}\text{O}_{2-x}$, $0.15 \leq x \leq 0.20$, but it is fugitive and difficult to see without practice.

Optically processed images

Optical enhancement of these weak contrast modulations was possible for those images whose

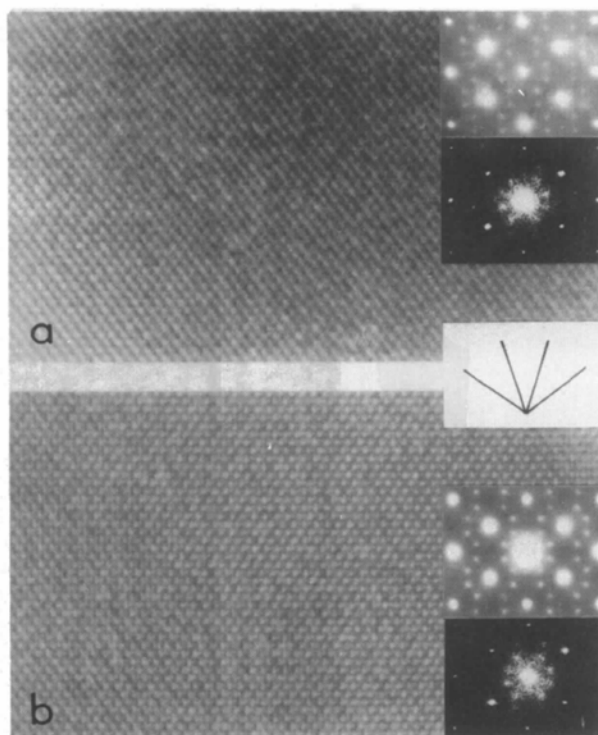


Fig. 5. High-resolution $[110]$ (cubic) images from (a) $\text{Ca}_{0.20}\text{Zr}_{0.80}\text{O}_{1.80}$ and (b) $\text{Ca}_{0.15}\text{Zr}_{0.85}\text{O}_{1.85}$, with corresponding electron diffraction patterns, and optical transforms. Weak fringes occurring in small patches may be seen if the images are viewed at low incidence in the directions indicated. The images have not been processed optically.

optical transforms showed a particularly favourable signal/noise ratio. For a micrograph magnification of 850000 and for light of wavelength 0.65×10^{-3} mm, Talbot self images of the [110] substructure spacing along the traces of (111) planes would be expected at successive 200 mm intervals of defocus, or at 100 mm intervals if lateral shifts of half a fringe are ignored.

Similarly, the very weak contrast fringes of spacing 5.4 and 6.2 Å would give Talbot self images at intervals of 324 and 427 mm. At these intervals the substructure contrast is largely attenuated, and the processed image shows the microdomains at maximum contrast (Fig. 6). An enlargement of an image taken at a defocus value such that the microdomain

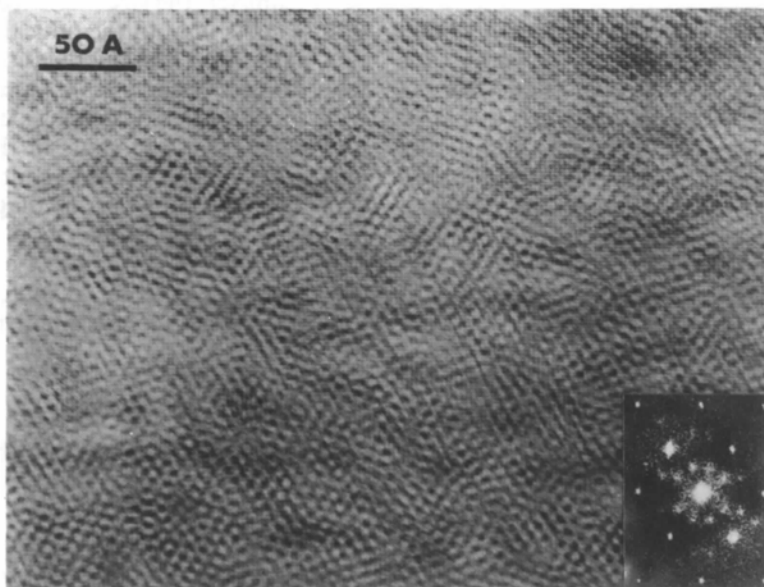


Fig. 6. Talbot image of a bleached micrograph from $\text{Ca}_{0.18}\text{Zr}_{0.82}\text{O}_{1.82}$ in [110] (cubic) orientation. The defocus value is such that the substructure is out of contrast, but the microdomain structure is at maximum contrast. The corresponding optical transform, when compared to those in Fig. 5, demonstrates the increased diffraction efficiency obtainable by bleaching the object micrograph, and yields a mean microdomain diameter of 28 Å for this specimen.

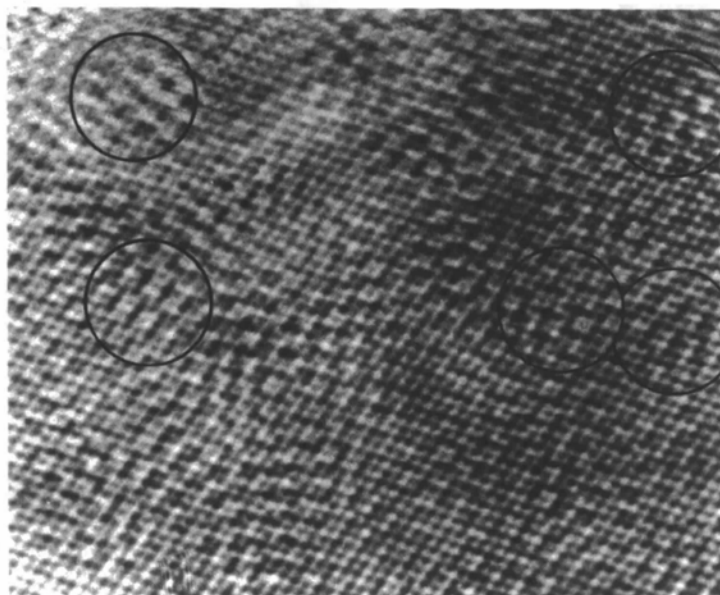


Fig. 7. Optically enhanced [110] image of $\text{Ca}_{0.18}\text{Zr}_{0.82}\text{O}_{1.82}$ from the same electron micrograph as in Fig. 6. Large numbers of microdomains exhibiting the 2-3 pattern of φ_1 in [010] or [010] orientation in various versions of contrast can be seen: some of these are indicated by circles whose diameter represents 30 Å.

contrast is high, whilst the substructure image is still visible, is shown in Fig. 7. The 2-3 patterns of φ_1 in [010] and [0 $\bar{1}$ 0] orientations can be recognized in many of the microdomains.

Microdomains of φ_1 structure have been identified only for two of the twelve possible orientations, but since images from a great variety of crystals in any orientation of the form $\langle 110 \rangle$ were essentially the same, it is clear that the microdomains must exist in all twelve orientations.

It would be expected that about one sixth of the volume of crystal imaged would consist of microdomains of φ_1 in the imageable orientations [010] and [0 $\bar{1}$ 0], so that the projected area of an imaged crystal of realistic thickness will show a much higher apparent density of such microdomains, and most imageable microdomains will be overlaid by various thicknesses of crystal that shows no superstructure contrast. Images (not shown) were calculated for composite structures composed of 29, 58 and 87 Å thicknesses of φ_1 in [010] orientation, each overlaid by increasing thicknesses of $\text{Ca}_{0.2}\text{Zr}_{0.8}\text{O}_{1.8}$ material of classical defect-fluorite structure in the same orientation as the subcell of the φ_1 (*i.e.* [$\bar{1}$ 10]). These images showed that the contrast differences of the dots in the 2-3 pattern of φ_1 would be attenuated to an undetectable level if the φ_1 was overlaid by fluorite of more than twice the thickness.

Fig. 8 shows a [110] image and corresponding diffraction patterns from a crystal of $\text{Ca}_{0.15}\text{Zr}_{0.85}\text{O}_{1.85}$ that had been prepared by quenching from 1970 K, then annealed at 1270 K for 1000 h. Growth of the

microdomains to about 200 Å diameter, and the corresponding sharpening of the diffuse diffraction features into festoons of spots, whose positions and intensities are calculable as due to φ_1 (Allpress & Rossell, 1975), is evident. The contrast within any domain in the image can be identified (and confirmed by calculation) as due to φ_1 in one of its four imageable orientations (see below).

Concluding remarks

The contrast observed in the foregoing electron micrographs and in the Talbot-enhanced images can be interpreted in terms of microdomains of φ_1 (CaZr_4O_9) of 28 Å diameter dispersed coherently throughout a crystal of room-temperature CSZ. These observations therefore support the description of Allpress & Rossell (1975) for the crystalline constitution of Ca-CSZ.

The observation that domains of φ_1 grow on annealing is further support for the existence of microdomains of the same structure. Even if the volume growth of the above 200 Å domains was linear with time, and ignoring the usual rate-determining nucleation step, the time to grow φ_1 microdomains to 30 Å diameter from supposedly undifferentiated fluorite phase at temperatures below about 1500 K (the region of stability for macroscopic φ_1 phase: see Fig. 1) would be a few hours. Since the materials spent only a few tens of seconds at these temperatures during cooling, it must be supposed that the microdomain description of the structure of

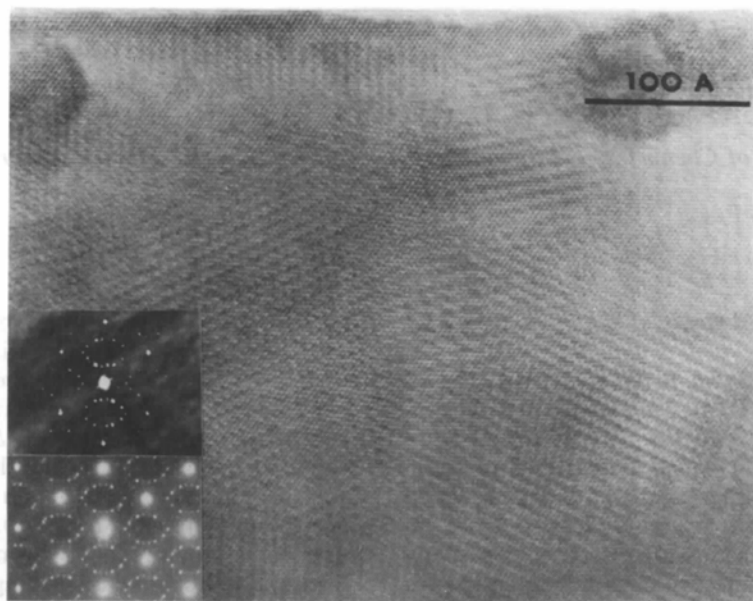


Fig. 8. Unprocessed high-resolution [110] image from $\text{Ca}_{0.15}\text{Zr}_{0.85}\text{O}_{1.85}$ annealed for 1000 h at 1270 K, with corresponding electron diffraction pattern, and optical transform. Relatively extensive domains are delineated by their contrast patterns, which are those expected for φ_1 in [010], [0 $\bar{1}$ 0], [$\bar{1}$ 02] and [10 $\bar{2}$] (supercell) orientations. Moiré fringes occur frequently when domains overlap.

the cubic phase applies at high temperatures, *i.e.* the presence of φ_1 microdomains is not an artefact produced during cooling.

The point would be decided by a high-temperature (>1500 K) diffraction experiment to see if the diffuse scattering was still present. This was carried out recently by Neder, Frey & Schulz (1990), who show that for single crystals of Ca_{0.15}Zr_{0.85}O_{1.85} at 1550 K, diffuse neutron scattering indeed occurs, and differs little from that observed at room temperature.

The authors gratefully acknowledge financial support from an Australian National University – CSIRO Collaborative Grant.

References

- ALLPRESS, J. G. & ROSSELL, H. J. (1975). *J. Solid State Chem.* **15**, 68–78.
- ALLPRESS, J. G., ROSSELL, H. J. & SCOTT, H. G. (1974). *Mater. Res. Bull.* **9**, 455–468.
- ALLPRESS, J. G., ROSSELL, H. J. & SCOTT, H. G. (1975). *J. Solid State Chem.* **14**, 264–273.
- CARTER, R. E. & ROTH, W. L. (1968). *Electromotive Force Measurements in High Temperature Systems*, edited by C. B. ALCOCK, pp. 125–144. London: Institute of Mining and Metallurgy.
- COWLEY, J. M. & MOODIE, A. F. (1960). *Proc. Phys. Soc.* **76**, 378–384.
- DWIVEDI, A. & CORMACK, A. N. (1990). *Philos. Mag. A*, **61**, 1–62.
- ETSHELL, T. H. & FLENGAS, S. N. (1970). *Chem. Rev.* **20**, 339–376.
- FILATOV, S. K. & FRANK-KAMENETSKII, V. A. (1969). *Kristallografiya*, **14**, 505–506.
- HELLMANN, J. R. & STUBICAN, V. S. (1983). *J. Am. Ceram. Soc.* **66**, 260–264.
- LEVIN, E. M. & MCMURDIE, H. F. (1975). *Phase Diagrams for Ceramists*. Columbus, Ohio: American Ceramic Society.
- MICHEL, D. (1973). *Mater. Res. Bull.* **8**, 943–950.
- MORINAGA, M., COHEN, J. B. & FABER, J. JR (1979). *Acta Cryst.* **A35**, 789–795.
- MORINAGA, M., COHEN, J. B. & FABER, J. JR (1980). *Acta Cryst.* **A36**, 520–530.
- NEDER, R. B., FREY, F. & SCHULZ, H. (1990). *Acta Cryst.* **A46**, 799–809.
- O'KEEFE, M. A. & BUSECK, P. R. (1979). *Trans. Am. Crystallogr. Assoc.* **15**, 27–46.
- ROSSELL, H. J. (1981). *Science and Technology of Zirconia, Advances in Ceramics*, edited by A. H. HEUER & L. W. HOBBS, Vol. 3, pp. 47–63. Columbus, Ohio: American Ceramic Society.
- ROSSELL, H. J., SELLAR, J. R. & WILSON, I. J. (1986). *Electron Microscopy*, Vol. 2. In *J. Electron Microsc.* **35**(Suppl.), 1667–1668.
- SHIOJIRI, M., HIROTA, Y., ISSHIKI, T., MAEDA, T. & SEKIMOTO, S. (1988). *Thin Solid Films*, **162**, 235–246.
- WILSON, I. J. (1985). *Opt. Acta*, **32**, 1497–1507.

Acta Cryst. (1991). **B47**, 870–881

Structure Refinement of Commensurately Modulated Bismuth Tungstate, Bi₂WO₆

BY A. DAVID RAE

School of Chemistry, University of New South Wales, PO Box 1, Kensington, New South Wales 2033, Australia

AND JOHN G. THOMPSON AND RAY L. WITHERS

Research School of Chemistry, Australian National University, GPO Box 4, Canberra, ACT 2601, Australia

(Received 19 February 1991; accepted 2 July 1991)

Abstract

The displacive ferroelectric Bi₂WO₆ [$M_r = 697.81$, $a = 5.4559$ (4), $b = 5.4360$ (4), $c = 16.4298$ (17) Å, $Z = 4$, $D_x = 9.512$ g cm⁻³, $Mo K\alpha$, $\lambda = 0.7107$ Å, $\mu = 958.6$ cm⁻¹, $F(000) = 1151.73$], is described at room temperature as a commensurate modulation of an idealized $Fmmm$ parent structure derived from an $I4/mmm$ structure. Transmission electron microscopy clearly showed that there are coherent intergrowths of two distinct modulated variants in Bi₂WO₆ crystals. Displacive modes of inherent $F2mm$ and $Bmab$ symmetry are substantial and coherent over a

large volume. They reduce the space-group symmetry to $B2ab$. A further substantial displacive mode corresponds to rotation of corner-connected WO₆ octahedra about axes parallel to c and has either of two inherent symmetries, $Abam$ or $Bbam$, the difference being associated with the way this mode propagates along c . The dominant $Abam$ mode reduces the space-group symmetry to $P2_1ab$, while the existence of the $Bbam$ mode reduces the intensity of $h + l = 2n + 1$ data and acts like a stacking fault. Group theoretical analysis of the problem details how the X-ray data can be classified so as to monitor the refinement. Anomalous dispersion selects the overall